Capacitive-based dilatometer cell constructed of fused quartz for measuring the thermal expansion of solids

J. J. Neumeier, R. K. Bollinger, G. E. Timmins, C. R. Lane,
R. D. Krogstad, and J. Macaluso
Department of Physics, P.O. Box 173840, Montana State University, Bozeman, Montana 59717-3840, USA

(Received 20 December 2007; accepted 31 January 2008; published online 13 March 2008)

A dilatometer cell that can detect sub angstrom changes in the length of solid specimens in the temperature range 5 K $< T <$ 350 K is described. It is constructed entirely from fused quartz (silica). This is a capacitive-based technique, where the spacing between two metallized plates allows detection of changes in length. It is also a relative measurement in the sense that the capacitor plate spacing is determined by the *relative* thermal expansions of the cell *and* sample. The advantage of using fused quartz is that it has among the smallest known thermal expansions. As a result, for most measurements, the sample's thermal expansion dominates the capacitance change. The construction and performance are described. It is directly compared to a dilatometer cell constructed of copper. Some thermometry and temperature control issues specific to dilatometry measurements are discussed. © *2008 American Institute of Physics.* [DOI: 10.1063/1.2884193]

I. INTRODUCTION

A wide range of techniques are applied in measuring the thermal expansion of solids. These are described in a number of publications.[1–4] This report is concerned with a capacitive-based thermal expansion cell (also referred to as a dilatometer cell). When the sample shrinks or expands, the capacitor gap d changes, which in turn changes the capacitance according to $C=\epsilon A/d$, where ϵ is the permittivity and A is the capacitor plate area. The sample is generally much larger than the capacitor gap and the sample is in thermal equilibrium with the cell. As a result, both the thermal expansion of the cell and that of the sample determine d. We refer to this type of measurement as *relative* since the thermal expansion of the sample relative to the material from which the cell is constructed determines the capacitance (clarified in Sec. III D). Therefore, the material of which the cell is constructed must be carefully chosen; ideally it should have the smallest possible thermal expansion. Most capacitive-based dilatometer cells are constructed of copper or copper alloys,[5–10] which have large thermal expansions. Capacitive-based cells constructed of materials with small thermal expansions, such as silicon[11] and fused quartz,[12] have been developed, but they have not been widely utilized in measuring the thermal expansion of solids.

Capacitive-based thermal expansion techniques have a number of advantages. Off-the-shelf capacitance bridges can measure with a resolution of about one part in 10^9, which translates to a typical sensitivity to changes in length of better than 0.1 Å. The size of the dilatometer cell can be small (about 8 cm^3). It is, in principle, possible to measure samples with lengths in the millimeter to centimeter range. Data can be collected continuously as the sample/cell temperature is varied. Measurements in magnetic fields are possible too. Some minor disadvantages exist as well. The thermal expansion of the material from which the cell is constructed must be well known in order to reliably subtract its contribution to the raw data. Also, an addendum must be measured and subtracted from the raw data; this is a measurement of the change in capacitance of the empty dilatometer cell (the *empty cell effect*). If the cell is made of an electrically conductive material, insulating spacers are needed to electrically isolate the capacitor plates. This can, in principle, lead to complicated differential thermal expansion effects and a large empty cell effect.

Here we introduce a dilatometer cell constructed from fused quartz (silica). The main advantage of this cell over copper cells lies with the extremely small thermal expansion of fused quartz, which leads to a smaller contribution of the cell's thermal expansion to the raw data (i.e., a smaller *relative effect*). A second advantage of the fused quartz cell lies in its very small empty cell effect. While the former makes the determination of the absolute thermal expansion of the measured sample more reliable, the latter enables measurement of samples with lengths as small as a few tenths of a millimeter. The basic design can be attributed to Kund.[12] We have improved the design, construction method, and assembly and developed a new sample mounting method. These changes have resulted in a significant reduction of the empty cell effect. Both the relative effect and empty cell effect are compared directly to those of a cell constructed of copper. We also discuss some aspects of thermometry and heating that are important for dilatometry measurements.

II. EXPERIMENTAL

A. Cell design, construction, and assembly

Over the 7 year duration of this project, numerous cell designs have been constructed and extensively tested. One design was shown in a recent publication.[13] These refinements, which will not be presented here, led to the design in Fig. 1. The cell is composed of five pieces. Two L-shaped

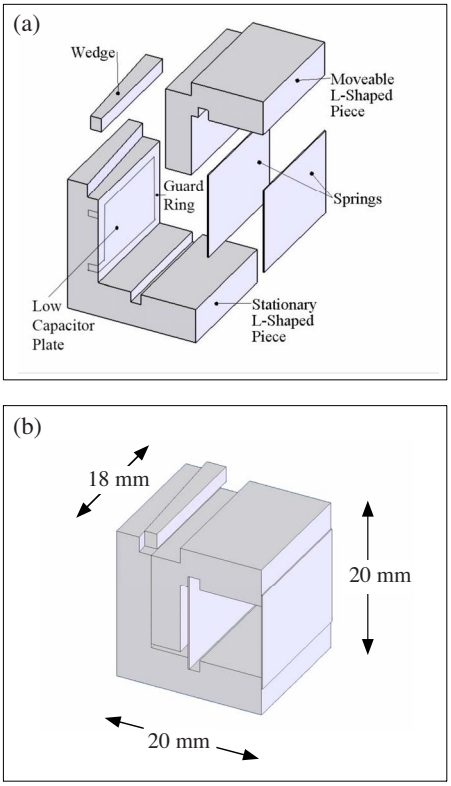

FIG. 1. (Color online) (a) Exploded view of the fused quartz dilatometer cell. (b) Assembled view of the cell.

pieces form the stationary and movable capacitor plates. On the vertical faces of the L-shaped pieces, a 100 Å/1000 Å Cr/Au film is deposited to form the metallic capacitor plates. The L-shaped pieces are joined with two fused quartz plates that are $12\times14\times0.14$ mm^3 in dimension; these act as springs. The springs are glued to the L-shaped pieces using a mixture of talcum powder and sodium silicate solution.[14,15] The stationary L-shaped piece has a cutout on the top with a 3° angle relative to the capacitor plate. The sample is placed on top of the movable plate and a wedge, also with a 3° angle, is pushed parallel to the capacitor plates to wedge the sample between it and the movable plate. This applies tension to the springs to establish the desired capacitor gap at room temperature. Figure 2 shows a sample mounted in one of our dilatometer cells. Wedges with a variety of widths are

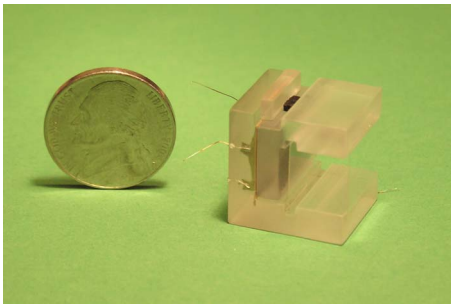

FIG. 2. (Color online) Assembled dilatometer cell with a sample installed. A US nickel (21.2 mm diameter) alongside the cell helps appreciate the size. The wires visible in the foreground are connected to the low capacitor plate and guard ring.

fabricated to accommodate samples of different lengths.

The L-shaped pieces are fabricated from a quartz ingot (Herasil I in these experiments)[16] using a surface grinder fitted with a resin-bonded diamond blade. The quartz work piece is fastened with Crystal Bond[17] to a flat plate of magnetic steel, which is held fast to the grinder via a magnetic chuck. The surface grinder spins at 3000 rpm, and the blades have diameters between 15 and 18 cm. Diamond blades of custom width were purchased for specific grinding tasks and a cup-shaped blade is used for the final finish of the capacitor plates; these possess diamond grits of 150 and 220, respectively. The grinding is done with a constant flow of water for cooling and no more than 25 μm is removed on one pass of the grinding wheel.[18] No polishing of the quartz parts was done although polishing of the regions where the springs are glued may improve adhesion.[15] Since it is important that the capacitor plates are parallel, extreme care is taken in the planning and execution of the grinding. Typical steps are as follows: (1) forming of a cube of quartz, (2) mounting on the grinder [from this point forward, it will not be removed until step (5) is complete], (3) grinding of the L piece to its approximate dimension, (4) finishing of the capacitor plate with the cup-shaped wheel so that it is perpendicular to grinding wheel axis, (5) grinding of the mounting surface of the spring that is furthest from the capacitor plate with the cup-shaped wheel (this also fixes the length of the L-shaped piece), and (6) grinding of the spring groove. At this stage, the part is repositioned on the machine for grinding of the 3° angle and sample mounting region. Generally, the two L-shaped pieces and the wedge can be fabricated in 3–5 days. Polished fused quartz wafers (20 Å roughness) with 100 mm diameter and 0.14 mm thickness were purchased. They were diced into rectangular plates (12×14 mm^2) for use as springs. All parts can be strain relieved at this stage by placing in a 10% HF acid solution for 1 min.

After the L-shaped pieces are finished, the Cr/Au film was vapor deposited to provide conducting surfaces with small tabs for electrical contacts. On the outer edge of one of the plates, about 1 mm from the edge, a guard ring is scratched into the surface to separate the low plate from the guard ring. During the experiment, the guard ring is grounded. This reduces fringe-field effects.[5,7] We constructed an *x-y-z* platform for scratching the guard ring. The tip of a phonograph stylus was glued to a piece of piano wire which was attached to the vertical (z) segment of the platform. The stationary (see Fig. 1) L-shaped piece was secured to the horizontal surface of the stage with double-sided tape. The guard ring was then carved with the stylus under a microscope.

Finally, the cell is assembled (see Fig. 2). We use a mixture of talcum powder and sodium silicate solution,[14] a glue that has been used for decades in the glass industry. This glue withstands high and cryogenic temperatures. A main advantage is that in the likely event that a spring breaks, the glue is easily dissolved by immersing the cell overnight in water. To make the glue, talcum powder is added to fresh sodium silicate solution forming a thick mixture that is then thinned 50:50 with water. We generally mix about 10 cm^3 and store it in a hypodermic needle for later use. An extensive study of

the fused quartz bonding process utilizing sodium silicate solution suggests some guidelines to improve the bond strength.[15] We have tested some of these ideas, such as eliminating the talcum powder from the glue, but at this stage cannot comment as to whether or not they provide any improvements in the decades-old method we have used for the bulk of this work. To glue the cell together, the two capacitor plates are held in intimate contact with CuBe springs; this guarantees parallelicity of the plates. The cell is stood on end, a spring is placed in the position furthest from the capacitor plate, and a small weight is placed on top. A small drop of glue is spread along the outer edge of the spring-cell joint and capillary action pulls it into the interface. After the glue dries, the spring closest to the capacitor plate is placed in position, a weight is placed on top, and it is glued at the four corners. Once the glue dries, the weight is removed and some glue is applied in the groove region. Under no circumstances should an excessive amount of glue be used or should glue be applied anywhere but to the outer edge of the spring-cell joint.

At this stage, 50 μm diameter annealed platinum leads are attached to the electrical tabs with silver paint. Short 90 μm copper leads are glued to the cell with the sodium silicate glue and soldered to the platinum leads (see Fig. 2). During experiments, the dilatometer cell is placed in a rectangular copper Faraday cage. The Faraday cage is permanently mounted on the end of a stainless steel tube with an o-ring flange on top. The high and low copper leads are soldered to the central conductor of two coax wires that exit the o-ring flange through hermetically sealed connectors. The ends of these coax wires are permanently mounted to the Faraday cage, near the dilatometer cell, to minimize noise from vibration and stray capacitance. The other copper lead, connected to the guard ring, is soldered directly to a ground tab inside the Faraday cage.

B. Cryostat

For the thermal expansion measurements, we use a helium cryostat with a custom designed insert that allows measurement in the range $5\ \mathrm{K} < T < 350\ \mathrm{K}$. The helium Dewar was purchased from a commercial source. It is a superinsulated Dewar, 1.2 m high, with a straight-bucket design that has an inside diameter of 15 cm and a liquid helium capacity of about 12 l. A flange was welded to the bottom so that the Dewar could be securely fastened to a massive disk of aluminum that has rubber vibration isolation feet on its bottom.

The insert has two concentric stainless steel tubes, one of 6.3 cm diameter and the other with 5.2 cm diameter. The space between these has layers of superinsulation; typically we place about 10 mbars of helium gas (at 295 K) in this space to provide thermal exchange with the helium bath. At the bottom of the inner tube, an oxygen free electrolytic (OFE) copper can with inside diameter of 4.7 cm and length of 17.5 cm is hard soldered. The copper can help provide an isothermal region for the dilatometer cell. We typically place 50 mbars of helium gas in this region at 295 K to promote thermal exchange. On the outside of the copper can, a 60 Ω heater made of manganin wire is glued with GE varnish.

C. Thermometry

During experiments, the Faraday cage is near the bottom of the copper can. Two thermometers are glued on a 2.5 mm thick slab of fused quartz that is held to the wall of the Faraday cage with springs fabricated from piano wire. The thermometers are at the same vertical height as the sample. We use an alumina-encased platinum resistance thermometer and a hermetically sealed high-temperature Cernox resistance thermometer. The Cernox (Ref. 19) has a larger dR/dT, where R is the thermometer's resistance, than platinum below ~220 K, above which platinum's larger dR/dT provides better sensitivity. They were calibrated in a Quantum Design Physical Properties Measurement System prior to installation (see below). A Lakeshore model 340 is used to measure the thermometer resistance during the dilatometry measurements. We found the firmware in this device inadequate to calculate the temperature from the resistance values since it only interpolates linearly between the calibration points.[20] Therefore, the calibration data are fit for entry into our LABVIEW program for the calculation of the temperature.

In calibrating the thermometers, the temperature was stabilized for 4 min before a resistance measurement was done. The Cernox excitation was 10 mV; the Pt thermometer excitation was 100 μA. The obtained resistance was an average of 25 resistance measurements. Data were collected from 2 to 375 K in 1.0 K increments.

The data for each thermometer were plotted as T vs R and fitted to a polynomial. The Cernox polynomial is of the form

$$T_{\mathrm{Cer}}(R) = a_0 R^{-5} + a_1 R^{-9/2} + a_2 R^{-4} + \cdots + a_{13} R^{3/2}. \quad (1)$$

The fit is valid in the range $2\ \mathrm{K} < T < 375\ \mathrm{K}$. For the Pt thermometer, the data were fitted to a polynomial of the form

$$T_{\mathrm{Pt}}(R) = b_0 R^{-8} + b_1 R^{-15/2} + \cdots + b_{23} R^{7/2}. \quad (2)$$

This particular fit is valid for the range $50\ \mathrm{K} < T < 375\ \mathrm{K}$. In both cases, the fitting was conducted using the least-squares routine in MATHEMATICA. These fits were entered into our LABVIEW data acquisition program for the calculation of the temperature during the dilatometry experiments.

In the LABVIEW program, the resistance for both thermometers are collected once every 50 ± 2 ms for the length of time required to produce one capacitance measurement (5.2 s). The resistances are converted to temperatures and a time stamp is provided by the computer, accurate to 1 ms. When the capacitance is obtained from the capacitance bridge, the time/temperature data are fitted to a straight line using LABVIEW's least-squares fitting routine. Approximately 104 data points for each thermometer will be fitted for any given C. The time of C is computed, and the T_{Cer} and T_{Pt} values corresponding to the C data point are found from the time/temperature fits.

The two temperatures thus obtained are then averaged by the following schemes:

$$\bar{T} = T_{\mathrm{Cer}}, \quad (3)$$

if $T_{\mathrm{Cer}} < 50$ K and

$$\bar{T} = [S_{Cer}T_{Cer} + S_{Pt}T_{Pt}]/[S_{Cer} + S_{Pt}], \quad (4)$$

for $50\ \mathrm{K} < T_{Cer} < 375\ \mathrm{K}$, where $\bar{T}$ is the mean temperature and $S=(dR/dT)$ for the respective thermometers.

The importance of smooth temperature calibration curves for thermal expansion measurements cannot be overemphasized. This lies with the fact that the thermodynamic quantity of interest, the thermal expansion coefficient μ, is the derivative of the measured relative change in length versus temperature [i.e., $\mu=(1/L_{300})(d\Delta L/dT)$]. As a result, any features or oscillations in the $T(R)$ fit will show up in μ. As a rule, after fitting the $T(R)$ data, we carefully inspect the first and second derivatives of the fits to ascertain their smoothness. This attention to the $T(R)$ fitting has led us to abandon spline interpolations, which are not as smooth as the fits given by Eqs. (1) and (2).

D. Heating routine

Prior to beginning a measurement, the inner cryostat tube is pumped with an oil-free turbopumping station for 12 h with three intermediate flushings with dry helium gas. The temperature of the dilatometer cell region is maintained at 350 K during the pumping; if this is not done, a noticeable upturn in the thermal expansion coefficient occurs near 300 K because of changes in the dielectric constant from desorbed gases. A typical vacuum at the end of this routine is 2×10^{-6} mbar. After pumping, approximately 50 mbars of helium gas is admitted to the dilatometer cell space to provide thermal exchange. Cryogenic fluid is then added to the Dewar, cooling the cell to the minimum temperature with this configuration (~5 K). At this stage, about 2 l of liquid helium are in the Dewar.

Once the dilatometer cell has reached its minimum temperature, current from the Lakeshore 340 is applied to the heater. We have developed a heating routine that operates within our LABVIEW data acquisition program. A key aspect is that the desired resolution for this experiment (typically 0.1 Å) requires that the warming rate remains constant. At present, the warming rate is held at 0.20(1) K/min for $5\ \mathrm{K} < T < 60\ \mathrm{K}$ and 0.200(2) K/min above 60 K. In the region near 40 K, where the liquid helium typically boils off, the rate may go briefly as high as 0.22 K/min. Our heating routine works in two modes. Below 20 K, a polynomial is used to ramp the heater power with time as the variable; this polynomial was determined empirically. Above 20 K, the warming rate is checked at a rate of 20 Hz and the power is increased only if the rate falls below 0.2 K/min.

III. EMPTY CELL EFFECT

A. Copper versus fused quartz for constructing dilatometer cells

Having explained the details of how our dilatometer cell is constructed and how the thermometry and heating are handled, we can move into actual measurements with the fused quartz cell. This is also a natural stage for comparing copper and fused quartz dilatometer cells. At present, copper is used almost universally as a construction material for capacitive-based thermal expansion cells. One reason for using fused quartz over copper has to do with the use of an electrically insulating versus electrically conducting material. If the latter is used, then insulating spacers are needed to electrically isolate the high and low capacitor plates from one another. Unfortunately, these insulating spacers are at critical positions in the cell. As a result, differential thermal expansion effects will occur that must be subtracted from any measurement data. This adds an additional contribution to the empty cell effect, which, ideally, should be due only to the thermal expansion of the capacitor plate area and the gap. If a thermal expansion cell is constructed of an electrically insulating material, such as fused quartz, no insulator is required to electrically isolate the capacitor plates; thus the empty cell effect should be better behaved and most likely smaller in magnitude. The empty cell effect is determined by measuring the capacitance versus temperature of the dilatometer cell with a piece of the material from which the cell is constructed in place of a sample.

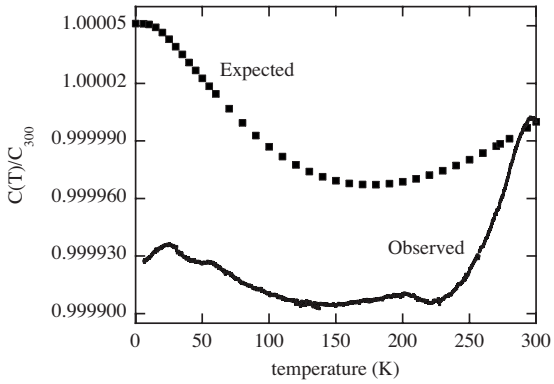

FIG. 3. Expected empty cell effect determined with Eq. (5) and that observed in measurements with our fused quartz dilatometer cell plotted as $C(T)/C_{300}$ vs T.

The second advantage of a fused quartz cell over one constructed of copper has to do with the very small thermal expansion of fused quartz. This leads to a far smaller contribution of the cell material to any measurement data (i.e., a smaller relative effect) over a large temperature range. However, at 27 K the thermal expansion coefficient magnitudes are equal for fused quartz and copper, and below this temperature, that of copper is smaller.[21,22] Thus, as far as the relative effect is concerned (see Sec. III D), there is no clear advantage of fused quartz over copper below 27 K.

B. Empty cell effect

We begin by evaluating the empty cell effect, which can easily be calculated. It is given by

$$C(T) = C_{300}(1 + \Delta L(T)/L_{300}), \quad (5)$$

where $C(T)$ is the temperature-dependent capacitance, C_{300} is the capacitance at 300 K, $\Delta L(T)/L_{300}$ is the linear thermal expansion of the material from which the cell is constructed (normalized to the length at 300 K, L_{300}), and $\Delta L(T)=L(T)-L_{300}$. Equation (5) is the ideal case scenario. It includes only the effects associated with the temperature-dependent capacitor plate area and gap.

Figure 3 shows the calculation using Eq. (5) and linear

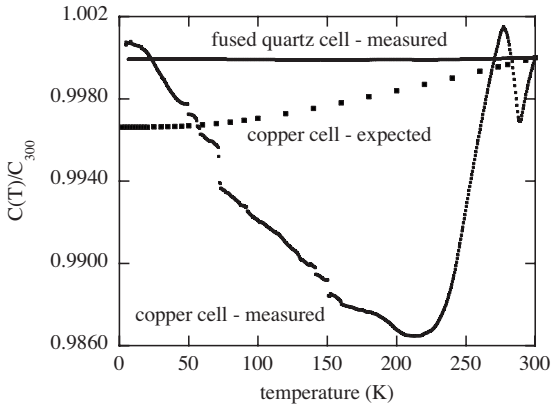

FIG. 4. The top curve is the measured empty cell effect for our fused quartz dilatometer cell. The middle curve is the expected empty cell effect for a copper dilatometer cell determined with Eq. (5) and the bottom curve is that observed in measurements with our copper dilatometer cell.

thermal expansion data for fused quartz.[21] These particular fused quartz data are used since they are determined from an *absolute* measurement rather than a relative measurement. In the latter, the thermal expansion of the material from which the cell was constructed would have been subtracted. Along with the expected empty cell effect, the observed effect is shown, as determined through measurements using the cell described herein. These data are typical of what we have observed for numerous cells. We believe that the discrepancy between the observed and expected curves is due to contributions from the glue and imperfect surfaces on which the springs are glued. At the onset of this project, our measured empty cell effect was more than 200 times larger than that shown in Fig. 3. This was due to an excessive amount of glue on the springs, which caused the springs to bend. The gluing method we have developed (Sec. II A) minimizes the amount of glue used, encourages a flat glue joint and flat spring, and thus minimizes the observed empty cell effect. Another source for the previously larger empty cell effect was the use of a CuBe spring to hold a fused quartz sample block (previously used instead of the quartz wedge) against the sample to maintain the sample position.[12,13] Due to the large thermal expansion of CuBe relative to fused quartz, this led to large and sometimes irreproducible features in the empty cell effect. The goal of eliminating any metal spring on the cell led us to the quartz wedge design.

It is instructive to compare the data in Fig. 3 to similar data for a thermal expansion cell constructed of copper. To realize this, we constructed a cell similar to that reported by Schmiedeshoff *et al.*[9] The details of this construction will not be discussed herein. Figure 4 illustrates this comparison by showing the measured empty cell effect for the fused quartz cell (topmost curve), the expected empty cell effect for a copper cell (middle curve) calculated using Eq. (5) and published linear thermal expansion data,[22] and the measured effect for our copper cell. Comparing the top two curves first, the expected empty cell effect for copper is 35 times larger than our measured effect for the fused quartz cell; the maximum magnitudes of $C(T)/C_{300}$ are used for this and the following comparison. The measured effect for the copper cell (lowest curve in Fig. 4) is 4 times larger than the expected effect and 140 times larger than our observed empty cell effect for the fused quartz cell. Furthermore, there are large discontinuous features in the data which can be difficult to reliably subtract from measurement data taken with a sample installed in the cell. We believe that these features and the large overall observed empty cell effect for our copper cell compared to the expected behavior can be attributed to differential thermal expansion effects. Most likely, these could be minimized through clever improvements in the design. However, the best empty cell effect for a copper cell will never be reduced to that of a cell constructed of fused quartz.

We take a moment to view the empty cell effects from the perspective of how large a correction they would be to typical measured ΔL values. For this, we make use of $\epsilon A = 1800$ pF μm and $C_{300}=15$ pF (see Sec. III C). For the fused quartz cell, the $C(T)/C_{300}$ values at 300 and 150 K (0.9999) can be used to calculate the correction in terms of a length from $\Delta L_{\mathrm{corr}}=1/C(T)-1/C_{300}$. This leads to the value $\Delta L_{\mathrm{corr}}=12$ nm. For our copper cell, an estimate using similar ϵA and C_{300} values but $C(T)/C_{300}$ at 215 K of 0.986 reveals $\Delta L_{\mathrm{corr}}=1.7$ μm. This value is more than 30% of the overall thermal expansion[13] of MgB_2 from $5\ \mathrm{K}<T<300$ K! The small empty cell effect of the fused quartz cell is an important advantage in determining the absolute thermal expansion of the sample, especially when the sample is small (where ΔL will also be small) or in the case of samples with small thermal expansions.

C. Calibration

In the course of this project, we have utilized two methods of calibrating the thermal expansion cell. The first is, ideally, devoid of any contribution from fused quartz itself. The procedure is as follows. After measuring the empty cell effect for one of our cells, we install a piece of annealed, high-purity, polycrystalline copper. Generally, this specimen is roughly 2 mm in length. We then measure the capacitance vs T from 5 to 300 K. Naturally, due to the relative effect, there is a contribution of fused quartz to these data. However, $\Delta L/L_{300}$ is zero at 300 *and* 79.3 K for fused quartz. As a result, there is *no* contribution of fused quartz to measurements at these two temperatures and the calibration routine reduces to, after subtraction of the empty cell effect, the adjustment of ϵA until the curve calculated via

$$\Delta L/L_{300} = (\epsilon A/L_{\mathrm{Cu}})(1/C(T) - 1/C_{300}), \tag{6}$$

overlaps the two points. In Eq. (6), L_{Cu} is the length of our copper sample at 300 K and C_{300} is the capacitance at 300 K. One of the reasons for choosing this method was to isolate our calibration from the published data for copper below 15 K, for which Kroeger and Swenson have noted[22] that there is no agreement among published results. Since the agreement at 300 and 79.3 K is reliable,[22–24] we only used these two temperatures. However, the maximum disagreement with the published $\Delta L/L_{300}$ data[22] is about 1% with this method; this is at 5 K. Most likely, this can be attributed to slight variations of the temperature where $\Delta L/L_{300}$ crosses zero for different varieties of fused quartz. We mention this method due to the novel approach and because future work

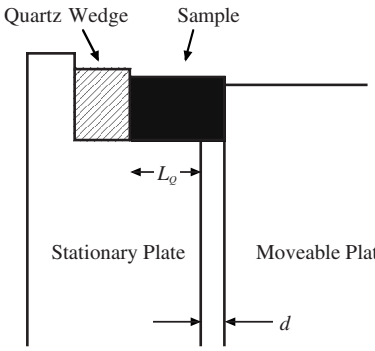

FIG. 5. Diagram illustrating the region of the cell near the sample. The right capacitor plate (movable plate) position is determined by the sample, while the left capacitor plate (stationary plate) position is determined by the thermal expansion of a length of quartz (L_Q) equal to the length of the sample minus the capacitor gap d.

might have better access to more precise data for specific types of fused quartz.

The second calibration method, which we currently use (after subtraction of the empty cell effect) is to adjust for the relative effect (see Sec. III D) and fit ϵA simultaneously to obtain the best possible fit to $\Delta L/L_{300}$ data for copper. Generally, an iterative approach would be used. This method yields $\Delta L/L_{300}$ data for our copper sample differing from the published $\Delta L/L_{300}$ data[22] by no more than 8×10^{-6} over the whole temperature range. Typical obtained values for ϵA are in the 1600–2000 pF μm range. In most experiments, we measure in the 10–20 pF range (d=200–100 μm).

D. Corrections due to thermal expansion of cell: The relative effect

Besides the empty cell effect, a very important aspect is the correction necessary to compensate for the thermal expansion of the cell itself. This can be best appreciated by the drawing shown in Fig. 5. We emphasize that the geometry in Fig. 5 is chosen for clarity, but the argument given below is valid for any geometry in which the cell and sample are in thermal equilibrium and the capacitor plates are parallel. The drawing illustrates the region near the sample. The capacitor gap d is determined by the separation between the movable capacitor plate (on the right) and the stationary capacitor plate (on the left). The position of the movable capacitor plate is clearly determined by the right side of the sample. However, the length L_Q in Fig. 5 will be determined *solely* by the linear thermal expansion of fused quartz. As a result, the linear thermal expansion of any sample must be adjusted for the thermal expansion of a length of fused quartz, $L_Q = L_S - d$, where L_S is the length of the sample. The correction is calculated with

$$L_Q(T) = L_Q^{300}(1 + \Delta L/L_{300}). \tag{7}$$

In Eq. (7), $\Delta L/L_{300}$ is the linear thermal expansion of fused quartz[21] and L_Q^{300} is the value of L_Q at 300 K. We refer to this as the relative effect. Furthermore, it should be clear from the diagram in Fig. 5 that one can never use a fused quartz cell to measure the thermal expansion of fused quartz.

The importance of this correction for the comparison of fused quartz and copper thermal expansion cells can *only* be appreciated by considering measurements of a sample other than copper. For this reason, we use measurements on MgB_2 which were published previously.[13] Figure 6 shows the gap of our thermal expansion cell versus temperature for actual measurements of a 4238 μm long sample of MgB_2. The curve which shows the smallest gap at 5 K is the data after subtraction of the empty cell effect. Correction for the thermal expansion of quartz (i.e., the relative effect) yields the curve which lies slightly above it at 5 K. Because of the fact that fused quartz initially contracts on cooling and then expands reaching the same length at 79.3 K as at room temperature,[21] the corrected data cross over the uncorrected data at 79.3 K. The top curve shows the expected gap if the same measurement was conducted in a copper thermal expansion cell. Because the thermal expansion of copper is roughly three times that of polycrystalline MgB_2, when the sample shrinks, the gap actually gets larger (see diagram in Fig. 5) as a result of the relative effect. This behavior was calculated using the published data[13] for MgB_2, the value d=101.8 μm at 300 K, and an equation identical to Eq. (7) with the published $\Delta L/L_{300}$ values[22] for copper. The data in this plot illustrate a distinct advantage of the fused quartz cell in that the correction for the thermal expansion of the material from which the cell is constructed (i.e., the relative effect) is 63 times smaller for fused quartz for the specific case of MgB_2.

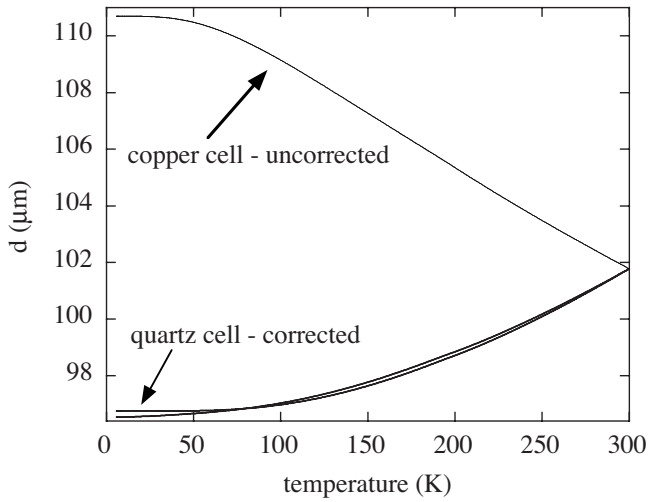

FIG. 6. The capacitor gap d vs T. Lowest curve (at 5 K) is the raw data (after correction for the empty cell effect) for the gap of our fused quartz dilatometer cell from measurements of a 4238 μm long sample of MgB_2. The curve just above (at 5 K) was corrected for the relative effect associated with the thermal expansion of fused quartz. The top curve represents the expected behavior if an identical sample was measured in a dilatometer cell constructed of copper; this curve includes the relative effect; no empty cell effect has been added.

IV. PERFORMANCE OF THE FUSED QUARTZ THERMAL EXPANSION CELL

Rather than use an excessive amount of space to illustrate the performance of the cell described herein, we refer to some recently published work and show one example of work in progress to highlight the utility of this device. The cell was used to investigate the critical behavior of a ferromagnetic phase transition[25] in $La_{0.7}Ca_{0.3}MnO_3$. Although the

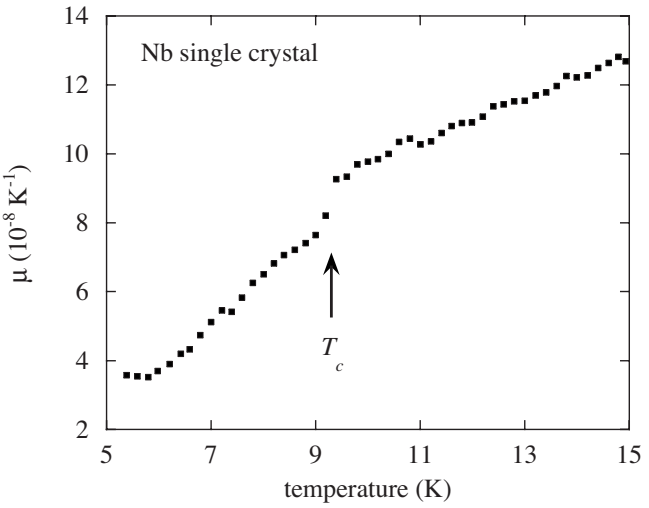

FIG. 7. Thermal expansion coefficient μ of a 10.818 mm long single crystal of Nb near the superconducting transition temperature T_c. Clearly evident is the jump in μ expected for a second-order phase transition.

feature in the thermal expansion coefficient μ at the ferromagnetic transition temperature T_c is quite large in this system, the need to have little scatter in the data as T_c is approached from above or below in order to determine the critical exponent α is challenging. The data shown in Fig. 3 of Souza *et al.*[25] were determined from a point-by-point derivative of $\Delta L/L$ and were *not* subjected to any smoothing. Finally, in this work, we evaluated a fundamental relation from thermodynamics which uses the overlap of μT and the heat capacity C_P to prove that the phase transition is continuous.

As noted above, the cell was used to measure the thermal expansion of the superconducting compound[13] MgB_2. We found that obtaining sufficient resolution to observe the normal to superconducting phase transition was especially challenging. In particular, special attention to grounding of the experimental system was essential in obtaining the 1×10^{-6} pF stability in our capacitance bridge that was required to yield subangstrom resolution. That resolution was indeed obtained as is evident in the inset of Fig. 3 in that publication.[13] Despite the excellent resolution of the $\Delta L/L$ data, obtaining the thermal expansion coefficient was more problematic because of the relative poor resolution of the temperature channel[26] and less than adequate control of our temperature ramping rate, which has improved since the time of publication. As a result, the $\Delta L/L$ data were carefully fitted with Chebyshev polynomials prior to taking the temperature derivative to determine μ. This procedure was described previously.[13]

More recently, we have measured the normal to superconducting phase transition of a 10.818 mm long single crystal of Nb. These measurements have incorporated the most recent improvements to the heating routing (Secs. II C and III D). Our approach in this case was to measure $\Delta L/L$ in the vicinity of T_c 14 times, differentiate each curve to obtain μ, and average *all* of the μ data sets.[27] The results are shown in Fig. 7. The jump in μ at T_c is expected for the second-order phase transition from the superconducting to the normal state. The ability to clearly observe the jump at T_c in a superconductor serves well to exemplify the high resolution of our dilatometry system since the effect is very small. Note that the jump in Nb is about 4.5 times smaller than the jump[13] in MgB_2.

Another investigation with this cell was the paramagnetic to antiferromagnetic phase transition[28] in $Na_{0.80}CoO_2$ and $Na_{0.75}CoO_2$. There we were able to observe the paramagnetic to antiferromagnetic phase transition and to determine the critical exponent α associated with the phase transition. Since the measured samples were single crystals, we were able to clearly observe the anisotropy in $\Delta L/L$ and μ in our data. In addition, we used the method reported previously[25] to show that the phase transitions are continuous.

Finally, we note our measurements of the thermal expansion of single crystalline $Li_{0.9}Mo_6O_{17}$, which is a well-known quasi-one-dimensional conductor.[29] The samples are platelet-like single crystals with very poor electrical conductivity out of the platelet plane. In this study, the two measured crystals had thicknesses of 0.523 and 0.308 mm; the thermal expansion for these lengths was easily determined with our fused quartz cell. This is a tribute to the small empty cell effect. The high planar electrical conductivity of this compound is dominated by zigzag Mo–O chains which lie along the *b* axis. Our thermal expansion data were able to show that the zigzag chains move closer together with cooling because of the large thermal expansion of the *a* axis. In fact, relative to the planar *b* and *c* axes, this distance contracts at least twice as strongly. This facilitates a crossover in dimensionality that leads to superconductivity at low temperature, a three-dimensional phenomenon.

V. CONCLUSION

This report has described our thermal expansion measurement system, the heart of which is a novel thermal expansion cell constructed entirely from fused quartz. There are two main advantages of this cell over cells constructed of copper. First, is that quartz is an electrical insulator, which alleviates the problem of electrically isolating the capacitor plates in copper thermal expansion cells. This leads to a far smaller empty cell effect. Second is the significantly smaller thermal expansion of fused quartz, which leads to a substantially smaller contribution to measurement data from the thermal expansion of the cell (i.e., a smaller relative effect). Furthermore, the cell is simple in design, being composed of only five parts. A number of recent measurements with cells of this design were highlighted. Some of the developments in this work could be applied in the construction of cells from other materials such as silicon[11] and sapphire, and for special applications, such as use in pulsed magnetic fields where eddy current heating could be limited by the use of an electrical insulator. We also presented aspects of thermometry and heating that are important to dilatometry measurements.

ACKNOWLEDGMENTS

We are especially thankful to Michael Kund and Klaus Andres for their assistance and encouragement during the early stages of this project and Michael Simmonds for his continued interest and assistance. We thank Michael

Hundley for his help in unraveling the problems with the Lakeshore 340 firmware. We have benefited from George Schmiedeshoff's sharing of his copper-cell design. Thanks to David Cebulla for making the drawings in Fig. 1, to Hugo Sandim for the Nb single crystal, and to Stan Tozer for the microcoax used in our Faraday cage. This material is based upon work supported by the National Science Foundation [Grant Nos. DMR-0301166 (and 9982834) (CAREER), DMR-0504769, DMR-0552458 (REU-Site), and DMR-0244058 (REU-Site)] and the U.S. Department of Energy Office of Basic Energy Sciences (Grant No. DE-FG-06ER46269). Partial financial support from Florida Atlantic University and Montana State University is gratefully acknowledged.

[1] T. H. K. Barron and G. K. White, *Heat Capacity and Thermal Expansion at Low Temperatures* (Kluwer Academic, New York, 1999).
[2] B. Yates, *Thermal Expansion* (Plenum, New York, 1972).
[3] S. Kanagaraj and S. Pattanayak, Cryogenics **43**, 399 (2003).
[4] K. Andres, Cryogenics **2**, 93 (1961); K. Andres and H. Rohrer, Helv. Phys. Acta **34**, 398 (1961).
[5] G. K. White, Cryogenics **1**, 151 (1961).
[6] G. Brändli and R. Griessen, Cryogenics **13**, 299 (1973).
[7] R. Pott and R. Schefzyk, J. Phys. E **16**, 444 (1983).
[8] M. Rotter, H. Müller, E. Gratz, M. Doerr, and M. Loewenhaupt, Rev. Sci. Instrum. **69**, 2742 (1998).
[9] G. M. Schmiedeshoff, A. W. Lounsbury, D. J. Luna, S. J. Tracy, A. J. Schramm, S. W. Tozer, V. F. Correa, S. T. Hannahs, T. P. Murphy, E. C. Palm, A. H. Lacerda, S. L. Bud'ko, P. C. Canfield, J. L. Smith, J. C. Lashley, and J. C. Cooley, Rev. Sci. Instrum. **77**, 123907 (2006).
[10] M. O. Steinitz, J. Genossar, W. Schnepf, and D. A. Tindall, Rev. Sci. Instrum. **57**, 297 (1986).
[11] R. Villar, M. Hortal, and S. Vieira, Rev. Sci. Instrum. **51**, 27 (1980).
[12] M. Kund, *Uniaxiale Effekte in Organischen und Keramischen Supraleitern* (Verlag Harri Deutsch, Frankfurt, 1995).
[13] J. J. Neumeier, T. Tomita, M. Debassai, J. S. Schilling, P. W. Barnes, D. G. Hinks, and J. D. Jorgensen, Phys. Rev. B **72**, 220505(R) (2005).
[14] E. V. Angerer, *Technische Kunstgriffe bei Physikalischen Untersuchungen* (Friedr. Vieweg and Sohn, Braunschweig, 1966), p. 59.
[15] E. J. Elliffe, J. Bogenstahl, A. Deshpande, J. Hough, C. Killow, S. Reid, D. Robertson, S. Rowan, H. Ward, and G. Cagnoli, Class. Quantum Grav. **22**, S257 (2005).
[16] Herasil I has since been replaced by Herasil 102 (see www.heraeusoptics.com).
[17] This product can be found at www.aremco.com.
[18] During grinding, the machine operator should wear a dust mask to protect against inhalation of the quartz mist, which could lead to silicosis.
[19] We use the Cernox thermometer with part No. CX-1070-SD because of its large dR/dT. The excitation level of 10 mV, higher than the recommended ranges, reduces thermometer noise.
[20] If one calculates the thermal expansion coefficient $\mu=(1/L_{300})(d\Delta L/dT)$ using temperature values interpolated with the Lakeshore 340 firmware, distinct steps in the data occur. This results from the 340's assumption that the temperature is linear between each set of two calibration points. Jumps were also evident in the data at each tabulated calibration point. We have not checked whether or not this naïve approach was improved upon in later firmware versions. This weakness aside, the Lakeshore 340 measures resistance with performance on par with modern voltmeter/current-source devices and its computer-controlled power supply has proven to be an excellent and stable source for the heater in this experiment.
[21] M. Okaji, N. Yamada, K. Nara, and H. Kato, Cryogenics **35**, 887 (1995); these data were extended above 273 K using data in Ref. 1.
[22] F. R. Kroeger and C. A. Swenson, J. Appl. Phys. **48**, 853 (1977).
[23] K. Wang and R. R. Reeber, High Temp. Mater. Sci. **35**, 181 (1996).
[24] M. Okaji, N. Yamada, H. Kato, and K. Nara, Cryogenics **37**, 251 (1997).
[25] J. A. Souza, Y.-K. Yu, J. J. Neumeier, and R. F. Jardim, Phys. Rev. Lett. **94**, 207209 (2005).
[26] While the capacitance bridge has a resolution of one part in 10^9, the Lakeshore 340 has a resistance resolution of one part in 10^5 or 10^6 depending on the resistance range. This has a major impact on the calculation of the thermal expansion coefficient $\mu=(1/L_{300})(d\Delta L/dT)$, leading to scatter in the data.
[27] R. K. Bollinger, C. A. M. dos Santos, H. R. Z. Sandim, and J. J. Neumeier (unpublished).
[28] C. A. M. dos Santos, J. J. Neumeier, Y.-K. Yu, R. K. Bollinger, R. Jin, D. Mandrus, and B. C. Sales, Phys. Rev. B **74**, 132402 (2006).
[29] C. A. M. dos Santos, B. D. White, Y.-K. Yu, J. J. Neumeier, and J. A. Souza, Phys. Rev. Lett. **98**, 266405 (2007).